IIETA International Information and Engineering Technology Association
Advancing the World of Information and Engineering

Journal of New Materials for Electrochemical Systems
Vol. 27, No. 3, September 2024, pp. 258-269
Journal homepage: http://iieta.org/journals/jnmes

Microstructural Analysis of Optimized Carbon Steel Cladding Using Response Surface Methodology and Genetic Algorithms

R. Yokeswaran[1*], V. Vijayan[1], M. Loganathan[2], T.S. Senthilkumar[1]

[1] *Department of Mechanical Engineering, K. Ramakrishnan College of Technology, Tiruchirappalli – 621 112, Tamilnadu, India*
[2] *Department of Mechanical Engineering, M. Kumarasamy College of Engineering, Karur – 639 113, Tamilnadu, India*

Corresponding Author Email: yokesys@gmail.com

https://doi.org/10.14447/jnmes./jnmes.v27i3.a11

Received: 11/01/2024
Accepted: 31/08/2024

Keywords:
cladding, regression, Genetic Algorithm, hardness, corrosion rate, penetration depth

ABSTRACT

In this study, an innovative approach has been employed to evaluate the cladding performance characteristics of medium carbon steel using super duplex stainless steel filler material. This research explores the effect of welding current, gas flow rate, and welding speed on key performance indicators such as hardness, corrosion rate, bead width, and penetration depth. The maximum hardness of 137.4 Hv, maximum bead width of 6.728 mm, maximum penetration of 2.016mm and minimum corrosion rate of 26.25 x 10-3 mils/year were observed in proposed sample. The primary objective is to establish the empirical relationship between dependent and independent variables to identify the optimal parameters for cladding process. To accomplish this, the RSM and GA optimization has been utilized for modeling and optimization, respectively. The regression models are subjected to GA optimization to identify the best dependent and independent variables were 84.95A current, 7.12 lpm gas flow rate and 74.42 mm/min weld speed. The findings demonstrate that the predicted empirical model output the experimental values validating our approach. In addition the cladding process delivers a significant contribution in the field of welding and provides valuable insights into this process. The SEM & OM analysis was carried out for optimized sample which microstructure is fine-grained also desirable for good weld quality.

1. INTRODUCTION

The act of cladding is a type of surface preparation process. Surfacing is the technique that uses a filler material to get deposited on top of another metal. This activity improves a special kind of property that is expected of the base material in addition to its original characteristics. Now-a-days it is used in the fabrication of engineering components in several industries like chemical, fertilizer, nuclear power plants, food processing, Petro chemical and their allied industries, agricultural machines and even in aircraft and missile components. The ultimate aim of this surfacing process is to inculcate the properties needed for specific applications from a specific metal without altering their basic nature. The selection of a suitable welding process for cladding a metal would be a very difficult task for industrial personnel. Hence in this study, a novel approach of using Tungsten Inert Gas (TIG) welding approach for cladding is followed. Due to less distortion. Because of low heat input carbon migration on clad surface is minimized and we need to produce less bead height. Hence TIG welding is chosen. NiCO3. The carbon steel filler material over the base metal of stainless steel during cladding. Local Hardening Zone (LHZ) formation with micro-hardness value of 425 HV1 was observed in the microstructural studies carried out on cladded samples due to the formation of martensite phase [1]. The coated duplex stainless steel on gray cast iron using inert shielding gas metal arc welding and Plasma Transferred Arc Surface Welding (PTA-SW). Artificial sea water corrosion was reduced owing to higher cooling and lower heat input conditions [2]. The mechanical properties of 316L plate cladded with Ni–Cr–Mo (ERNiCrMo-3) alloy using TIG welding operation. Properties of corrosion resistance and creep strength were evaluated for the cladded surface. Hardness was improved to 260 HV0.5 at cladding, 208 HV0.5 at interface and 205 HV0.5 at base material. Lower heat input combination is the reason for improving the corrosion rate as Niobium does not segregate successfully at this temperature level. Dendrites in the form of column and cellular structures were observed at the area closer to the cladding zone in the microstructure analysis [3]. The optimal damper positioning under earthquake conditions. The Genetic Algorithm (GA) approach was coupled with Abaqus software to develop models for structural building applications. The results indicated that the parallel processing of Finite Element Analysis (FEA) results from Abaqus with the GA yields accurate results [4]. The GA in face milling operation carried out on brass material with HSS cutter. The operation

was carried out following the Orthogonal Array (OA) L27 design of experiment with input parameters of spindle speed, feed and depth of cut. Output responses measured were Material Removal Rate (MRR) and Surface Roughness (SR). Combined objective function was formulated using the weighting function approach and provided to GA as an objective function. The output of GA had been obtained as the best possible outcome. The GA solver was executed in C++ solver with necessary operating conditions [5]. GA in face milling of copper and brass material as work piece. RSM was used to develop relationship between the input and output in the form of mathematical models. Best result (optimal machining parameters) was attained with the aid of GA approach. Reduction in peak loads was achieved through GA with an error of 4%. Input parameter significance on output was studied by the analysis of variance [6]. The Genetic Algorithm (GA) approach for optimizing the process parameters chosen in order to achieve the best response possible for different machining operation such as turning, welding, drilling, milling, etc [7-15].

RSM technique for analyzing the surface roughness generated during the turning operation carried out on 42CrMo4 hardened steel with the tool material of Al2O3/TiC mixed ceramic cutting tool [16]. RSM to predict and find the optimized results for reduced wear in the proposed composite matrix. Further the properties of hardness and fracture toughness were improved along with wear resistance [17].Compared and analyzed the carbon steel and stainless steel as filler metal in welding of stainless steel clad carbon steel. The microstructure results showed that austenite grains were high in stainless steel filler but martensite was found in carbon steel filler [18].The deposited WC-10Co-4Cr on the surface of AISI-304 stainless steel using TIG welding process to improve the wear resistance further Mathematical models were developed for predicting the results with a confidence level of 95% [19,20,21]

In summary, cladding is a surface preparation process used in various industries to improve the properties of a base metal without altering its basic nature. Tungsten Inert Gas (TIG) welding is a suitable method for cladding due to its low heat input and minimized carbon migration on the clad surface. Several studies have used the Genetic Algorithm (GA) approach for optimizing the process parameters in different machining operations such as turning, welding, drilling, and milling. In the current study, TIG welding using L9 Orthogonal array has been employed for cladding a metal, and tests are conducted to evaluate the clad zone, corrosion rate, bead width, and penetration depth. The results are analyzed using regression analysis and the GA approach to obtain the best possible outcome. Also the SEM and OM analysis has been studied for the optimized result.

2. MATERIALS AND EXPERIMENTAL WORK

Several metals are available on the surface of Earth and not all of them can be used for any kind of applications. Only few alternatives shall be used for the process of high temperature operations owing to factors such as hardness, yield strength, corrosion resistance, thermal resistance, etc. The material chosen for the analysis in this work is IS2062 medium carbon steel, containing 0.26% carbon by weight percentage. The clad / filler material which is coated on the IS2062 medium carbon steel is chosen as SS2594 super duplex stainless steel. Similarly to workpiece, the filler material is chosen for the reason that it possesses good corrosion resistance upon high temperature application.

The TIG weld cladding process is described in this chapter. The process parameters involved in the procedure was described. Here, the cladding was carried out at different combination of operating parameters chosen for experimentation. The chosen variables and their levels are mentioned as well.

2.1 Tungsten Inert Gas Weld Cladding Process

Process of improving the surface hardness and resistance towards corrosion was set to be the aim of this study. For the process of cladding, Tungsten Inert Gas (TIG) Weld cladding was utilized. The schematic layout of actual experimental set up is shown in Figure 1 (Fig. 1).

2.2 Experimental Design

The full factorial design was initially used by many researchers to understand the effects of process parameters on the operation conducted in various materials during the early days. After the advent of Genichie Taguchi, the concept of orthogonal arrays and reduced experimental design were introduced. This made a great change in the industrial approach by reducing the large amount of money and time invested during the testing period for newer materials and machining processes. Here as well, Taguchi's L9 Orthogonal Array (OA) is followed. The Table 1 provides the actual value for each factor as per the L9 orthogonal array design developed in Table 2.

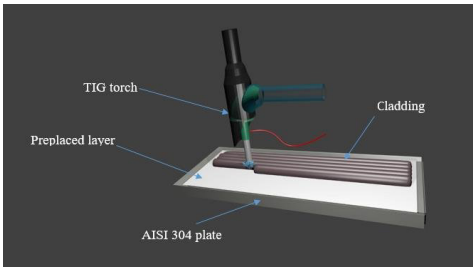

Figure 1. Schematic layout of TIG welding setup and cladding process

Table 1. Process Parameters and Their Levels

Process parameters	Unit	Levels		
		-1	0	1
Current	A	80	110	140
Gas Flow Rate	lpm	4	6	8
Welding speed	mm/min	38	45	70

Table 2. Experimental design in terms of actual value for parameters

Experimental run	A: Current (A)	B: Gas flow rate (lpm)	Weld speed (mm/min)
1	80	4	38.18
2	80	6	38.89
3	80	8	39.62
4	110	4	42.00
5	110	6	46.15
6	110	8	48.84
7	140	4	68.85
8	140	6	70.00
9	140	8	75.00

3. RESULTS AND CONCLUSION

The RSM - GA results were proposed on the basis of its prediction. The proposed RSM model was validated with 9 experimental data of full factorial design that used for the L9 orthogonal array experimental design. The predicted values of hardness, corrosion rate, bead width, penetration depth were validated with the respective experimental values and the percentage of error is presented in Table 3 according to the experimental and theoretical investigation, discussions are made as follows

3.1 RSM for Average Clad Zone Hardness

The maximum hardness of 3600HRC occurs at the specific combination of gas flow rate and current due to the underlying mechanism of the process of hardening is shown in Figure 2 (Fig. 2). Hardening is a heat treatment process used to increase the hardness of a material, such as steel, by heating it to a specific temperature and then rapidly cooling it down, typically in a quenching bath. The rapid cooling causes the material to undergo a structural transformation, forming a hard and brittle martensitic microstructure.

In the case of gas quenching, a gas is used to rapidly cool the material instead of a liquid quenching bath. The gas flow rate and current are two important parameters that determine the cooling rate during the hardening process. At a low gas flow rate and high current, the cooling rate is slower, which can result in a less hard and more ductile microstructure. On the other hand, at a high gas flow rate and low current, the cooling rate is faster, which can result in a more brittle and less ductile microstructure.

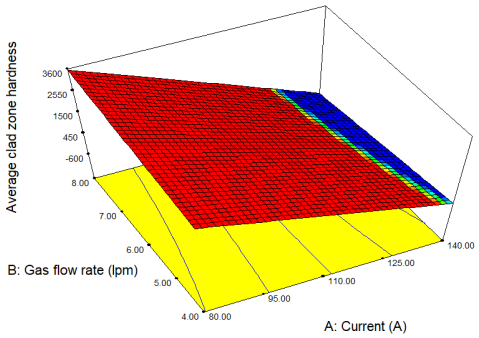

Figure 2 Response surfaces of average clad zone hardness vs. Current & Gas flow rate

Table 3. Experimental design in terms of actual value for parameters with Results

Experimental run	Current (A)	Gas flow rate (lpm)	Weld speed (mm/min)	Average clad zone hardness	Corrosion rate (10^-3 mils/year)	Width (mm)	Penetration Depth (mm)
1	80	4	38.18	137.26	26.25	4.561	0.01
2	80	6	38.89	128.73	34.33	5.057	0.0012
3	80	8	39.62	134.80	28	6.728	0.001
4	110	4	42.00	130.60	43.41	5.085	0.95
5	110	6	46.15	134.80	34.4	6.859	1.139
6	110	8	48.84	134.80	28	4.445	0.76
7	140	4	68.85	134.80	42.63	6.139	2.016
8	140	6	70.00	135.40	44.29	5.374	1.698
9	140	8	75.00	136.09	54.72	6.187	1.399

Therefore, the specific combination of a gas flow rate of 8 lpm and a current of 80A likely results in the optimal cooling rate for the material being hardened, leading to the formation of the maximum amount of martensite and thus the maximum hardness of 3600HRC.

In welding, a high-temperature heat source, such as an electric arc, is used to melt and join two or more pieces of metal. The weld metal undergoes a phase transformation during solidification and cooling, resulting in changes in the microstructure and mechanical properties of the weld. The welding speed and current are two important parameters that affect the cooling rate and solidification behavior of the weld.

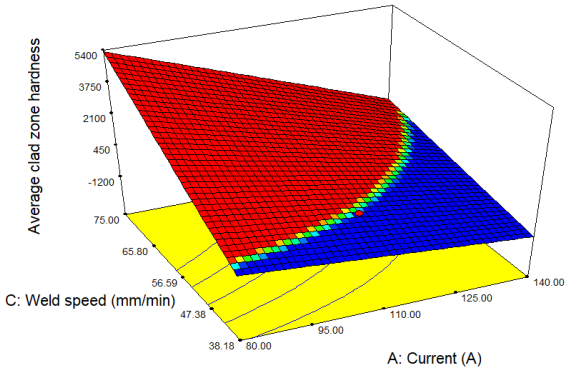

Figure 3. Response surfaces of average clad zone hardness vs. Current &Weld speed

At a low welding speed and high current, the heat input into the weld is high, resulting in a slower cooling rate and a larger heat-affected zone (HAZ) surrounding the weld is shown in Figure 3 (Fig. 3). This can lead to the formation of a coarse-grained microstructure with lower hardness.

On the other hand, at a high welding speed and low current, the heat input into the weld is low, resulting in a faster cooling rate and a narrower HAZ. This can lead to the formation of a fine-grained microstructure with higher hardness. Therefore, the specific combination of a welding speed of 75mm/min and a current of 80A likely results in the optimal cooling rate and solidification behavior for the specific material being welded, leading to the formation of the maximum amount of fine-grained microstructure with the highest hardness of 5400HRC.

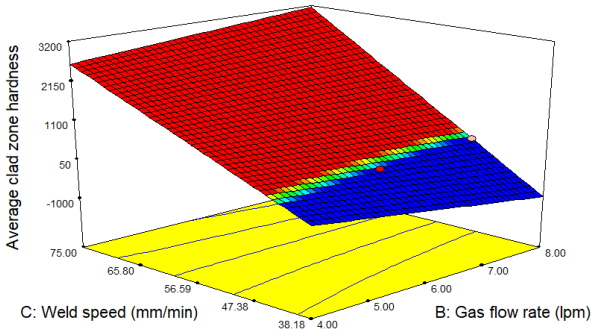

Figure 4. Response surfaces of average clad zone hardness vs. Gas flow rate & Weld speed

The maximum hardness of 3200HRC is likely due to a combination of factors that are influenced by the welding speed and gas flow rate is shown in Figure 4 (Fig. 4). At a lower welding speed of 38.18mm/min, the heat input per unit length of the weld is increased, which can result in a higher cooling rate of the weld pool. This rapid cooling rate can cause the formation of a finer microstructure, with a higher density of dislocations and defects, which can contribute to an increase in hardness.

In addition, at a higher gas flow rate of 8 lpm, the shielding gas provides better protection to the weld pool, preventing the formation of oxides and other contaminants. This can lead to a cleaner and more homogeneous microstructure, which can also contribute to an increase in hardness. However, it is important to note that the optimal welding parameters, including the welding speed and gas flow rate, can vary depending on the specific materials being welded and the welding process being used. Therefore, it is important to carefully select and optimize the welding parameters to achieve the desired properties in the final welded specimen.

3.2 RSM for Corrosion Rate

The maximum corrosion rate value of 30 x 10-3 mils/year is likely caused by a combination of electrochemical and chemical processes. The maximum gas flow rate of 8 lpm and maximum current of 140A can increase the rate of these processes, leading to a higher corrosion rate shown in Figure 5 (Fig. 5). When metal is exposed to a corrosive environment, such as in the presence of oxygen and water, it can undergo an electrochemical reaction known as oxidation. This reaction results in the formation of metal ions and the release of electrons. The electrons flow from the metal to the cathode, and the metal ions combine with other ions or molecules in the environment to form corrosion products.

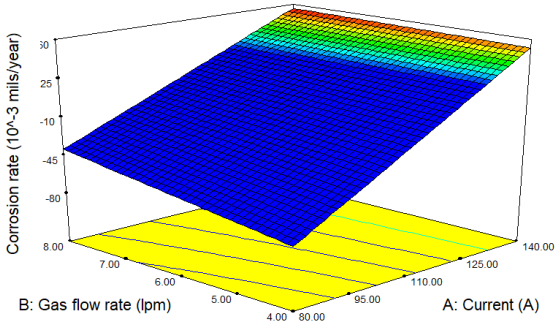

Figure 5. Response surfaces of Corrosion rate vs. Current & Gas flow rate

In addition to the electrochemical reaction, the gas flow rate can increase the rate of corrosion by promoting the diffusion of corrosive species to the metal surface. This can occur because a higher gas flow rate can create more turbulence and promote more mixing, leading to a higher concentration of corrosive species at the metal surface. The current also plays a role in corrosion rate, as it can influence the electrochemical reaction. When a current flows through a metal, it can accelerate the oxidation reaction by providing an additional source of electrons for the reaction [22]. This can lead to a higher rate of metal ion formation and, ultimately, a higher rate of corrosion. Therefore, the combination of high gas flow rate, high current, and exposure to a corrosive environment can increase the rate of electrochemical and chemical processes, leading to a higher corrosion rate.

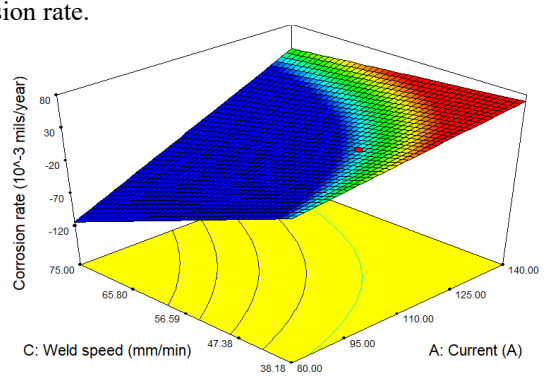

Figure 6. Response surfaces of Corrosion rate vs. Current & Weld speed

The maximum corrosion rate value of 80 x 10^{-3} mils/year is likely caused by a combination of factors, including the welding process itself, the composition of the material being welded, and the environmental conditions in which the welding is taking place. One possible mechanism behind this high corrosion rate is that the welding process is generating a high level of heat, which can cause the metal to undergo changes in its microstructure. These changes can create regions of the metal that are more susceptible to corrosion, leading to a higher corrosion rate.

The low welding speed of 38.18mm/min may also be a contributing factor shown in Figure 6 (Fig. 6). A slower welding speed can lead to longer exposure times for the metal in the high-temperature zone of the welding process, increasing the likelihood of changes in microstructure and thus increasing the susceptibility to corrosion. The high current of 140A can also contribute to the high corrosion rate by accelerating electrochemical reactions at the metal surface. As mentioned in the previous answer, when a current flows through a metal, it can accelerate the oxidation reaction by providing an additional source of electrons for the reaction. This can lead to a higher rate of metal ion formation and, ultimately, a higher rate of corrosion.

Finally, the environmental conditions in which the welding is taking place may also be a factor. For example, exposure to a corrosive gas, such as oxygen or chlorine, can increase the likelihood of corrosion. The high temperature of the welding process can also accelerate chemical reactions that promote corrosion. Overall, the combination of high temperature, low welding speed, high current, and exposure to a potentially corrosive environment can lead to a high corrosion rate.

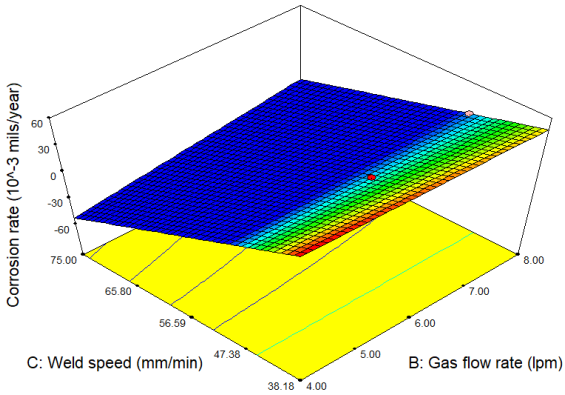

Figure 7. Response surfaces of Corrosion rate vs. Gas flow rate & Weld speed

The maximum corrosion rate of 60 x 10-3 mils/year is likely caused by a combination of factors, including the welding process, the composition of the material being welded, and the environmental conditions in which the welding is taking place. The low gas flow rate of 4 lpm may be a contributing factor to the high corrosion rate. A low gas flow rate can create an environment that is depleted in protective gases, such as argon, which are often used in welding to shield the weld from oxygen and other corrosive species. Without this protection, the metal is more vulnerable to corrosion.

Similarly, the low welding speed of 38.18 mm/min can also contribute to the high corrosion rate shown in Figure 7 (Fig. 7). A slower welding speed can lead to longer exposure times for the metal in the high-temperature zone of the welding process, increasing the likelihood of changes in microstructure and thus increasing the susceptibility to corrosion. The combination of low gas flow rate and low welding speed can also contribute to the accumulation of heat in the welding zone, which can create regions of the metal that are more susceptible to corrosion.

The environmental conditions in which the welding is taking place may also be a factor. For example, exposure to a corrosive gas, such as oxygen or chlorine, can increase the likelihood of corrosion. The high temperature of the welding process can also accelerate chemical reactions that promote corrosion. Overall, the combination of low gas flow rate, low welding speed, and exposure to potentially corrosive environmental conditions can lead to a high corrosion rate.

3.3 RSM for Bead Width

The maximum value of bead width of 8mm is likely caused by a combination of factors, including the welding process, the composition of the material being welded, and the environmental conditions in which the welding is taking place. The high current of 140A can contribute to the maximum value of bead width by providing more heat to the welding process. This increased heat can result in a larger heat-affected zone and greater melting of the metal, which can lead to a wider bead width.

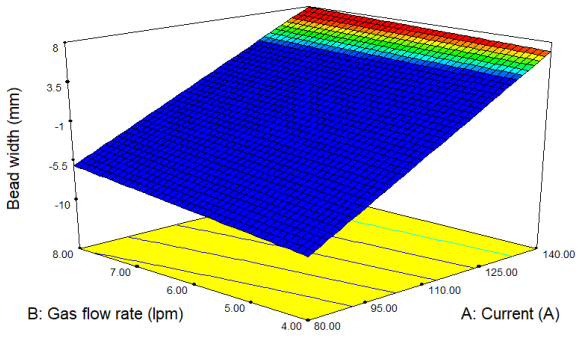

Figure 8. Response surfaces of bead width vs. Current & Gas flow rate

The high gas flow rate of 8 lpm can also contribute to the maximum value of bead width by promoting greater heat dissipation and shielding of the weld shown in Figure 8 (Fig. 8). The gas flow can help to cool the welding zone and remove contaminants that could interfere with the welding process. This results in a more consistent and uniform weld, which can lead to a wider bead width. In addition to these factors, the welding speed, voltage, and electrode size can also influence the bead width. For example, a slower welding speed can result in a wider bead due to the longer exposure time to the heat source. Similarly, a higher voltage can increase the amount of heat generated, which can lead to a wider bead.

Overall, the combination of high current and high gas flow rate, along with other welding parameters, can promote greater heat input, improved shielding, and a more consistent welding process, resulting in a wider bead width.

The maximum bead width value of 11mm is likely caused by a combination of factors, including the welding process, the chemistry of the material being welded, and the environmental conditions in which the welding is taking place. The high current of 140A can contribute to the maximum bead width by providing more heat to the welding process shown in Figure 9 (Fig. 9).

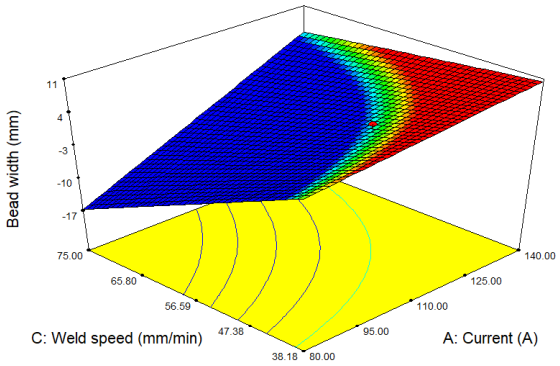

Figure 9. Response surfaces of bead width vs. Current & Weld speed

This increased heat can result in a larger heat-affected zone and greater melting of the metal, which can lead to a wider bead width.The low welding speed of 38.18 mm/min can also contribute to the maximum bead width by allowing for a longer exposure time of the heat source to the metal. This extended exposure time can result in more complete melting of the metal and a wider bead width.

In addition, the type of electrode used in the welding process can also influence the bead width. For example, a larger electrode diameter can lead to a wider bead width due to the increased amount of metal that can be melted and deposited.Overall, the combination of high current, low welding speed, and other welding parameters, along with the potential influence of environmental factors, can promote greater heat input, longer exposure time, and more complete melting of the metal, resulting in a wider bead width.

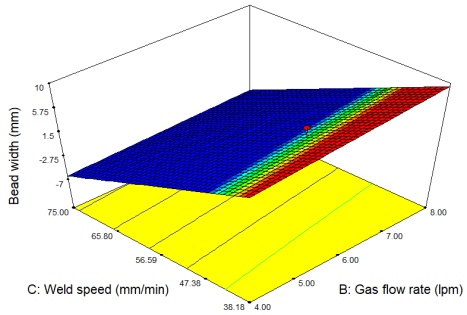

Figure 10. Response surfaces of bead width vs. Gas flow rate & Weld speed

The maximum bead width value of 10mm is likely caused by a combination of factors, including the welding process, the composition of the material being welded, and the environmental conditions in which the welding is taking place. The high gas flow rate of 8 lpm can contribute to the maximum bead width by promoting greater heat dissipation and shielding of the weld Figure 10 (Fig. 10). The gas flow can help to cool the welding zone and remove contaminants that could interfere with the welding process. This results in a more consistent and uniform weld, which can lead to a wider bead width. The low welding speed of 38.18 mm/min can also contribute to the maximum bead width by allowing for a longer exposure time of the heat source to the metal. This extended exposure time can result in more complete melting of the metal and a wider bead width.

In addition, the type of electrode used in the welding process can also influence the bead width. For example, a larger electrode diameter can lead to a wider bead width due to the increased amount of metal that can be melted and deposited.Overall, the combination of high gas flow rate, low welding speed, and other welding parameters, along with the potential influence of environmental factors, can promote greater heat input, longer exposure time, and more complete melting of the metal, resulting in a wider bead width.

3.4 RSM for Penetration Depth

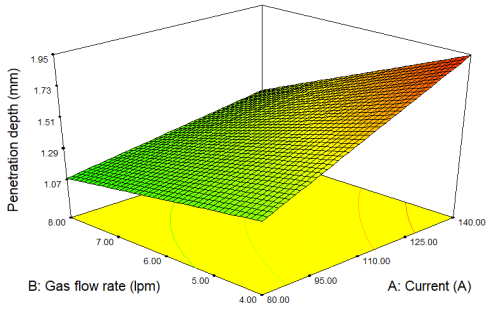

Figure 11. Response surfaces of penetration depth vs. Current & Gas flow rate

The maximum penetration depth of 1.95mm is likely due to a combination of factors, including the increased heat generated by the maximum current of 140A anssd the reduced gas flow rate of 4 lpm shown in Figure 11. (Fig. 11) When a high current is applied to a welding or cutting process, it increases the heat input to the material, which can result in deeper penetration. However, if the gas flow rate is too high, it can cause turbulence and interfere with the welding process, reducing penetration. Therefore, a lower gas flow rate can help to maintain stability and control the heat input to the material, leading to deeper penetration.

Additionally, the reduced gas flow rate can also result in a narrower and more focused arc, which can increase the energy density at the welding point, leading to deeper penetration. Overall, the combination of a high current and a low gas flow rate can create the conditions necessary for maximum penetration depth.

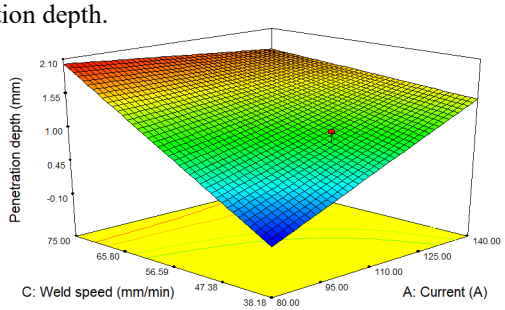

Figure 12. Response surfaces of penetration depth vs. Current & Weld speed

The maximum penetration depth of 2.10mm is likely due to the combination of the minimum current of 80A and the minimum weld speed of 38.18 mm/min Shown in Figure 12 (Fig. 12). When the current is low, the heat input to the material is also

reduced, which can result in deeper penetration due to the slower rate of heat dissipation. The slower weld speed allows more time for the heat to be absorbed by the material, which can also contribute to deeper penetration. At lower current levels, the arc is narrower and more concentrated, resulting in a higher energy density at the welding point. This can increase the depth of penetration by melting and fusing the material more effectively.

The slower weld speed can also contribute to deeper penetration by allowing more time for the material to melt and flow together, resulting in a larger weld pool and deeper fusion. Overall, the combination of the low current and slow weld speed creates the conditions necessary for maximum penetration depth, by allowing more time for heat to be absorbed by the material and for the material to melt and flow together.

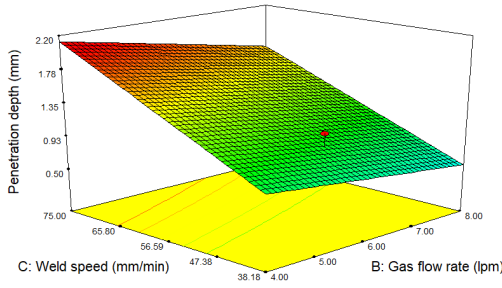

Figure 13. Response surfaces of penetration depth vs. Gas flow rate & Weld speed

The maximum penetration depth of 2.20mm is likely due to the combination of the minimum gas flow rate of 4 lpm and the maximum weld speed of 75 mm/min Shown in Figure 13 (Fig. 13). When the gas flow rate is low, it reduces the amount of shielding gas in the welding area, which can lead to a more stable and focused arc. This can create a higher energy density at the welding point, resulting in deeper penetration. The higher weld speed can also contribute to deeper penetration by creating more frictional heat between the welding tool and the workpiece. This can increase the temperature and fluidity of the material, allowing it to melt and flow more easily and resulting in deeper fusion.

Furthermore, the combination of the low gas flow rate and high weld speed can create a "keyhole" effect during welding, where the welding tool penetrates deeply into the material and leaves a narrow channel or "keyhole" behind it. This can increase the depth of penetration by exposing more of the material to the heat source and allowing it to melt and fuse together. Overall, the combination of the low gas flow rate and high weld speed can create the conditions necessary for maximum penetration depth by increasing the energy density at the welding point and allowing the material to melt and flow more easily. The keyhole effect can also contribute to deeper penetration by exposing more of the material to the heat source.

3.5 Regression Analysis

This work tried to make mathematical relationship between independent variables of current, gas flow rate, and welding speed and with dependent variables of hardness, corrosion rate, and bead width and penetration depth. In sense the regression analysis id=s used to make a relationship.

$$\begin{aligned} Average\ \ clad\ \ zone\ \ hardness\ \ &= -8845.3134\ \ + 77.1083\ \ \times A + 67.1779\ \ \times B \\ &+ 210.6595\ \ \times C - 6.1249\ \ \times A \times B - 1.6181\ \ \times A \times C + 9.8619\ \ \times B \times C \end{aligned} \quad (1)$$

Equation (1) provides a regression equation for predicting the hardness value of a cladded sample with an R-squared value of 0.9988 and a Pred R-squared value of 0.9953. The 'Pred R-squared' value of 0.98 was reasonably close to the 'Adj R-squared' value of 0.98. The value of the equation's 'Adeq Precision' is 46.237, which is higher than 46.237(Expected). As a result, this model can be utilized to analyze the design space in question. The reading's standard deviation and mean were found to be 4.38 and 275.87, respectively. The equation could be used to predict the hardness of cladded samples with ease (1). The R-squared value is 0.9988, and the projected values are shown in Figure14(Fig. 14) in comparison. This equation's confidence level was set at 99 percent, with only a 1% margin of error permitted. The confidence level is higher than 95%, indicating that there is only minor variation. As a result, within the operating range of experimentation, the same can be utilised to forecast the findings.

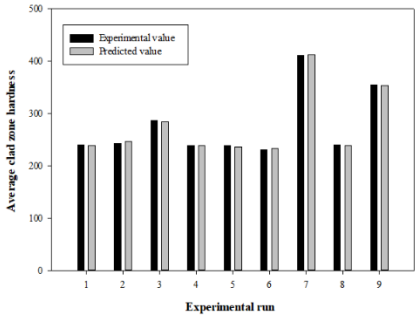

Figure 14. Validation of regression model for average clad zone hardness

$$\begin{aligned} Corrosion\ \ rate\ &= 1.7348 \times A + 0.3583 \times B - 2.7323 \times C - 0.2789 \times A \times B \\ &- 0.0014 \times A \times C + 0.5681 \times B \times C \end{aligned} \quad \textbf{(2)}$$

The equation (2) with R-squared value of 0.9959 and Pred R-squared value of 0.9416 might be used to determine the corrosion rate of cladded samples. The reading's standard deviation and mean were found to be 4.207 and 37.34, respectively. The 'Pred R-squared' value was 0.9879, which was in close agreement with the 'Adj R-squared' value. The value of the equation's 'Adeq Precision' is 7.227, which is more than 4. (Expected). As a result, this model can be utilised to investigate the design space.

The equation could be used to forecast the corrosion rate of cladded samples with ease (2). In Figure15 (Fig. 15), the R-squared value is 0.9959, and predicted values are compared. This equation's confidence level was set at 99 percent, with only a 1% margin of error permitted. The confidence level is greater than 95%, and it can be used to forecast results within the experimentation's operational range.

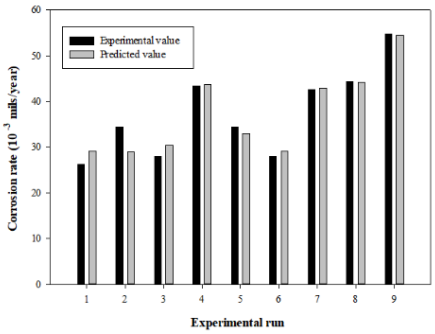

Figure 15. Validation of regression model for corrosion rate

$$Bead\ width = 0.0419 \times A + 1.2027 \times B - 0.0454 \times C - 0.0098 \times A \times B \quad (3)$$

Equation (3) shows the regression equation for predicting the bead width value of cladded samples, with an R-squared value of 0.9936 and a Pred R-squared value of 0.9421. The 'Pred R-squared' value was 0.9631, which was in reasonable agreement with the 'Adj R-squared' value. The value of the equation's 'Adeq Precision' is 12.6543, which is more than 4. (Expected). As a result, this model can be used to investigate the design space. The reading's standard deviation and mean were found to be 1.088 and 5.603, respectively.The equation might be used to predict the bead width of cladded samples with ease (3). In Figure 16 (Fig. 16), the R-squared value is 0.9936, and the predicted values are compared. The confidence level for this equation was 96 percent, with only a 4% margin of error permitted. The confidence level is greater than 96 percent, and it can be used to forecast results within the experimental operating range.

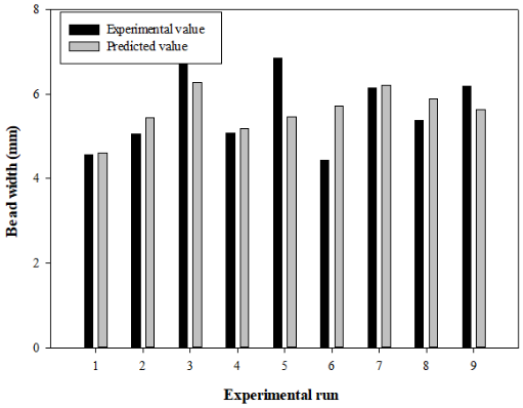

Figure 16. Validation of regression model for bead width

$$Penetration\ depth = -3.5476 + 0.0474 \times A + 0.2074 \times B - 0.0085 \times C - 0.0024 \times A \times B \quad (4)$$

The equation (4) with R-squared value of 0.9862 and Pred R-squared value of 0.9487 could simply be used to determine the penetration depth of cladded samples. The reading's standard deviation and mean were found to be 0.1266 and 0.8847, respectively. The 'Pred R-squared' value was 0.9723, which was in reasonable agreement with the 'Adj R-squared' value. The value of the equation's 'Adeq Precision' is 21.2676, which is more than 4. (Expected). As a result, this model can be utilised to investigate the design space. The equation could be used to predict the penetration depth of cladded samples with ease (4).

In Figure17 (Fig. 17), the R-squared value is 0.9862, and predicted values are compared. The confidence level for this equation was 94 percent, with only a 6% margin of error permitted. The confidence level is greater than 90%, and it can be used to forecast results within the experimentation's operational range.

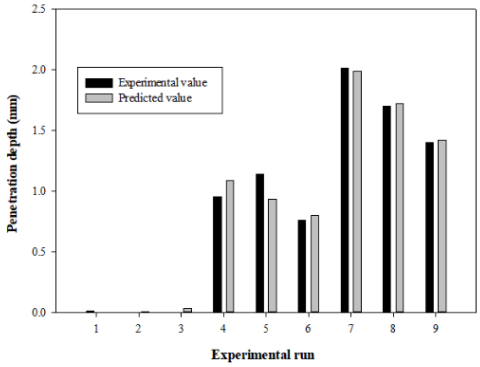

Figure 17. Validation of regression model for penetration depth

3.6 Genetic Algorithm Optimization for Process

The optimization process was carried out using a code created specifically for the Genetic Algorithm technique, which was based on concepts obtained from natural genetics dynamics to identify the optimal answer for the given problem. In Table 4, the prerequisites for the procedure to run were clearly stated. Microsoft Visual C++ was used as the solver. In this experiment, the population size and the number of iterations were both set to 100. The roulette search optimization function was used as the selection function. The mutation probability was set to 0.1, and the cross-over probability at 0.9. The binary single point function was used as the cross over type, and the switching approach was 1 point cross-site type. The convergence on the response was arrived following the strategy of sharing on parameter space option.

Table 4 Parameter setting for GA optimization code

Sl. No.	Parameter	Value
1	Population type	Double vector
2	Population Size	100
3	Iteration	100
4	Cross over type	Binary Single point
5	Cross over function	0.8
6	Stall generation	100

By using weight function allocation, the independent multiple goal functions were unified into a single objective function throughout this optimization. Hardness was given a weight of 0.33, corrosion rate was given a weight of 0.33, bead width was given a weight of 0.17, and penetration depth was given a weight of 0.17. Table 5 shows the upper and lower bounds of the process parameter values for the optimization code to run. The optimal solution was obtained by combining the GA code with this limiting restriction. Table 6 shows the optimum findings that were obtained.

Table 5. Lower and upper bounds of process parameter setting for GA optimization code

Sl. No.	Parameter	Lower bound value	Upper bound value
1	Current (A)	80	140
2	Gas Flow Rate (lpm)	4	8
3	Welding speed (mm/ min)	38	75

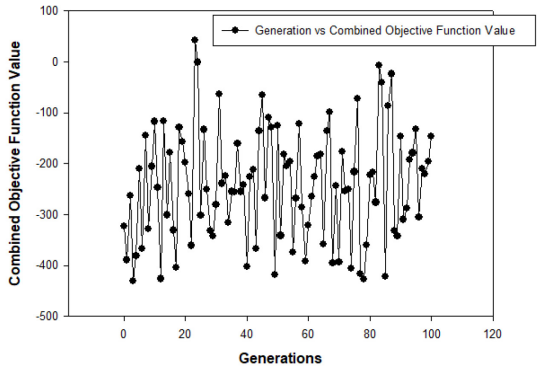

Figure 18 Optimized values for the combined objective function using Genetic Algorithm

The combined objective function values acquired from the 100 iterations were displayed in Figure18(Fig. 18). The best result was reached after the third iteration. The value of the independent variable was determined by examining the rankings assigned during the iterations. Within the third iteration, optimised results were obtained by identifying the combination with the highest rank. The optimal values for the formulated combined objective function were known as the relevant values. Current = 84.95 A; Gas Flow Rate = 7.12 lpm; Welding speed = 74.42 mm/min; and total value = 1540.49 were the optimal values.

Table 6. Optimized process parameter setting obtained from GA

Sl. No.	Parameter	Value
1	Iteration number	3
2	Objective function value	1540.49
3	Current	84.95 A
4	Gas Flow Rate	7.12 lpm
5	Welding speed	74.42 mm/min

3.7 METALLURGICAL ANALYSIS OF OPTIMIZED PARAMETER SAMPLE

3.7.1 Microstructure Analysis

The microstructure taken with the help of Optical microscope was presented in the Figure 19(Fig. 19). Based on the images (a) & (b), it is clear that the grains were oriented along the direction of weld with minimal deviations. This improves the linear characteristics of the welded samples. This occurred owing to the proper selection of cladding parameters in the TIG welding process.

The Figure 19 (Fig. 19) (d) – (f) depicts a clear representation of uniformly distributed grains along with the direction of weld. The grain size was also very uniform within the cladded zone and heat affected zone. Columnar dendrite structure was observed from the results obtained (shown in (a) & (b)).

This was achieved by the equal heat transfer in all directions of the base material. The grains were very uniformly distributed by the influence of current and voltage applied during the cladding process. The presence of ferrite in the clad zone decreased with increase in heat input at the optimized parameters. This yielded defect less cladded surface of the base material. The grain size depicts the basic mechanical properties such as strength and corrosion characteristics of any metal. Here, the fine grain structure had improved the hardness of the surface without compromising the base material properties [23].

3.7.2 SEM Analysis

The SEM images were taken for the optimized sample after proper polishing and suitable surface preparation. At a magnification of 54X, the different layers were clearly visible (shown in Figure 20) (Fig. 20). The cladded material SS2594 duplex stainless steel formed a very smooth layer on top of the base material IS2062. The interface layer shows no sign of any defects. Further details could be observed from Figures 21 & 22 (Fig. 21&22), which show the SEM images taken at magnifications of 500X & 2 kX respectively

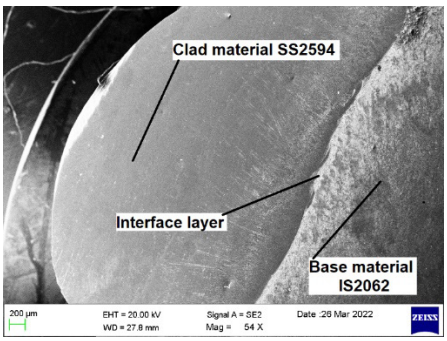

Figure 20. SEM image of clad sample at 54X (Optimized parameters)

The SEM image shows that the clad material is well-bonded to the base material. The interface layer is very thin, which indicates that there was good fusion between the two materials. This is important for preventing cracking and ensuring that the weld is strong.

The fine-grained microstructure of the clad material is also desirable for good weld quality. This microstructure is typically achieved by cooling the weld metal rapidly. Rapid cooling produces small, equiaxed grains, which are less likely to crack than large, elongated grains.

The SEM image overall shows that the cladded carbon steel weld is of good quality. The microstructure is fine-grained, the clad material is well-bonded to the base material, and the interface layer is thin. This indicates that the welding process was performed correctly and that the weld is likely to be durable and reliable.

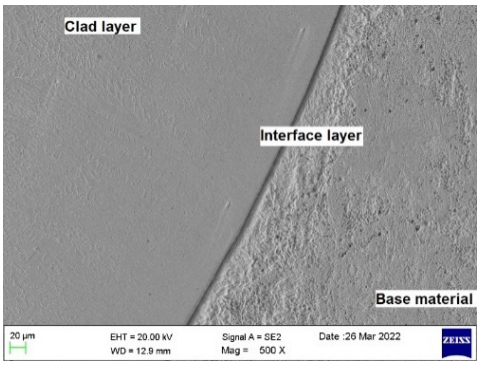

Figure 21. SEM image of clad sample at 500X (Optimized parameters)

The Figure 21 shows that the cladded carbon steel weld has a good microstructure. This indicates that the welding process was performed correctly and that the weld is likely to be of good quality. The interface layer is a thin layer of material that forms between the clad and base materials during the welding process. This layer is typically composed of a mixture of the clad and base materials. The thickness of the interface layer depends on the welding parameters used, but it is typically very thin (less than 5 micrometers). The welding parameters used to create cladded carbon steel welds are important for ensuring the quality of the weld. The current, gas flow rate, and welding speed must be carefully controlled to produce a weld with good microstructure and mechanical properties. [24]

The SEM image figure 22 (Fig. 22) shows that the clad and base materials are well-bonded together. The interface layer is very thin, which is desirable for good weld quality. The clad material has a fine-grained microstructure, which is also desirable for good weld quality. The interface layer in the SEM image is thin and uniform. This is desirable for good weld quality, as it helps to prevent the formation of cracks [24].

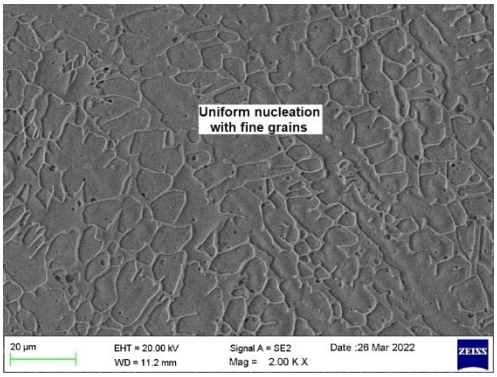

Figure 22. SEM image of clad sample at 2000X (Optimized parameters)

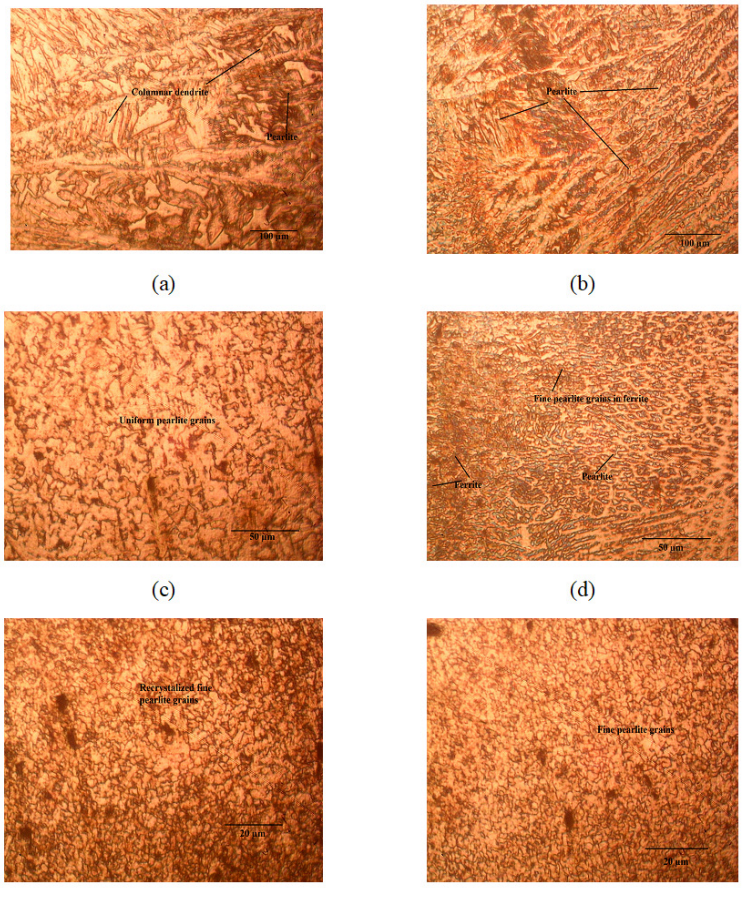

Figure 19 Optical microstructure results of cladded samples (optimized parameters)

4. CONCLUSION

At lower inert gas medium environments, higher values of hardness were recorded while the welding current was at its maximum[18].

Current, weld speed, and their combined effect all had an impact on corrosion rate.

Current, weld speed, and interactions between current – gas flow rate and current – weld speed all had an effect on bead width.

Current and the relationship between current and gas flow rate influenced penetration depth.

The poor cooling rate of argon shielding was caused by the thermophysical feature of a decreased convective heat transfer coefficient. As a result, a fine grain structure with a large number of nucleation was obtained in the cladded zone.

The regression equations with R-square values of 0.9988, 0.9959, 0.9936, and 0.9862 were created to predict the findings. The model's confidence level is set at around 95%, with only a modest margin of error.Predicted outcomes were used to validate the same.

The goal of the optimization was to find the input settings that would allow the average clad zone hardness, bead width, and penetration depth to be maximised while the corrosion rate of the cladded samples was minimised.

The optimal process parameters based on attractiveness were assessed to be 140 A current, 4 lpm gas flow rate, and 68.83 mm/min weld speed using Design Expert software. Average clad zone hardness was determined to be 411.45, with 41.3499 x10-3 mils/year, 1.99 mm bead width, and 5.81073 mm penetration.

The Genetic Algorithm was run on acombined output function that was weighted appropriately for each of the responses.
84.94118 A current, 7.12157 lpm gas flow rate, and 74.41961 mm/min weld speed were the GA optimised results. For the third generation, the combined objective function had a value of 1540.491.

The OM analysis of the optimized sample depicted uniformly distributed grains along with the direction of weld. The grain size was also very uniform within the cladded zone and heat affected zone.

Columnar dendrite structure was achieved by the equal heat transfer in all directions of the base material. The grains were very uniformly distributed by the influence of current and voltage applied during the cladding process.

The SEM analysis revealed a remarkably even coating on the clad surface, achieved through the use of an optimized sample. There are no indications of defects in the interface layer.

Conflict of interest:

On behalf of all authors, the corresponding author states that there is no conflict of interest.

REFERENCES

[1] Li, C *et al.*, Microstructures and mechanical properties of stainless steel clad plate joint with diverse filler metals, Journal of Materials Research and Technology. Korea Institute of Oriental Medicine, vol. 9, no. 2, pp. 2522–2534, (2020). DOI:10.1016/j.jmrt.2019.12.083

[2] Heider, B., Oechsner, M., Reisgen, U. et al. Corrosion Resistance and Microstructure of Welded Duplex Stainless Steel Surface Layers on Gray Cast Iron. J Therm Spray Tech 29, 825–842 (2020). DOI:10.1007/s11666-020-01003-y

[3] Evangeline, A., Sathiya, P. & Arivazhagan, B. Laves Phase Formation and Segregation of Nb in Ni–Cr–Mo Superalloy over 316L by Hot Wire (HW) TIG Cladding Process. Arab J Sci Eng 45, 9685–9698 (2020). DOI:10.1007/s13369-020-04873-0

[4] Thiyagarajan, K., Jayaraman, M., Vijayan, V., Ramkumar, R. (2020). Cluster analysis of lost foam casted Al-Zn-Mg-Cu alloy with K–Mean algorithm. Journal of New Materials for Electrochemical Systems, Vol. 23, No. 1, pp. 45-51. DOI:10.14447/jnmes.v23i1.a09

[5] Kannan, S., N. Baskar, M. Varatharajulu, and B. Suresh Kumar. " Optimization of Face Milling Parameters for Material Removal Rate and Surface Roughness on Inconel 718 using Response Surface Methodology and Genetic Algorithm." Asian Journal of Research in Social Sciences and Humanities 6(9):1198. DOI:10.5958/2249-7315.2016.00864.9

[6] Sathish, T., Chandramohan, D., Vijayan, V., Sebastian, P.J. (2019). Investigation on microstructural and mechanical properties of Cu reinforced with Sic composites prepared by microwave sintering process. Journal of New Materials for Electrochemical Systems, Vol. 22, No. 1, pp. 5-9. DOI:10.14447/jnmes.v22i1.a02

[7] Xu, D., and Ananthasuresh, G. K., Freeform Skeletal Shape Optimization of Compliant Mechanisms,ASME. J. Mech. Des. 125(2): 253–261 (2003). DOI:10.1115/1.1563634

[8] Santer, M., & Pellegrino S, Topological optimization of compliant adaptive wing structure. AIAA journal, 47(3), 523-534 (2009). DOI:10.2514/1.36679

[9] Vigneshwaran N.K. | Vishnu Prabhu S | Vignesh Kumar S | Ricordey Arumaidoss F, Effect of Contributing Parameters over Material Removal Rate in Machining Incoloy 825 using Electric Discharge Machining (EDM) , (ijtsrd) 1(6). 821-824 (2017). DOI:10.31142/ijtsrd4609

[10] Afrand, M., Esfe, M. H., Abedini, E., & Teimouri, H, Predicting the effects of magnesium oxide nanoparticles and temperature on the thermal conductivity of water using artificial neural network and experimental data. Physica E: Low-dimensional Systems and Nanostructures, 87, 242-247 (2017). DOI:10.1016/j.physe.2016.10.020

[11] A.P. Markopoulos, E.L. Papazoglou, P. Svarnias, P. Karmiris-Obratański, An Experimental Investigation of Machining Aluminum Alloy Al5052 with EDM, Procedia Manufacturing, Volume 41, 2019, Pages 787-794, DOI:10.1016/j.promfg.2019.09.071.

[12] Dao, T. P., Tran, N. T., Trang, T. N., & Ha, C. N., Prediction of Fatigue Life for a New 2-DOF Compliant Mechanism by Clustering-Based ANFIS Approach. Mathematical Problems in Engineering Volume 2021(14). DOI:10.1155/2021/6672811

[13] Gardan, N., & Schneider A., Topological optimization of internal patterns and support in additive manufacturing. Journal of Manufacturing Systems, 37, 417-425 (2015). DOI:10.1016/j.jmsy.2014.07.003

[14] Gardan, N. and Schneider, A.,Topological optimization of internal patterns and support in additive manufacturing. Journal of Manufacturing Systems, 37, pp.417-425 (2015). DOI:10.1016/j.jmsy.2014.07.003

[15] Carvalho, J. E. S. P., Sotomayor, P. O., Parise, J. A. R., &Pradelle, F., Numerical assessment of critical properties of nanofluids: Applications to nanorefrigerants and nanolubricants. Journal of Molecular Liquids, 318, 113938 (2020). DOI:10.1016/j.molliq.2020.113938

[16] Loganathan, M., Dinesh, S., Vijayan, V., Karuppusamy, T., Rajkumar, S. (2020). Investigation of mechanical behaviour on composites of Al6063 alloy with silicon, graphite and fly ash. Journal of New Materials for Electrochemical Systems, Vol. 23, No. 1, pp. 36-39. DOI:10.14447/jnmes.v23i1.a07

[17] Singh, J., Thakur, L., & Angra, S., A study of tribological behaviour and optimization of WC-10Co-4Cr Cladding. Surface Engineering, 37(1), 70-79 (2021). DOI:10.1080/02670844.2020.1745367

[18] Singh, J., Thakur, L., & Angra, S., An investigation on the parameter optimization and abrasive wear behaviour of nanostructured WC-10Co-4Cr TIG weld cladding. Surface and Coatings Technology, 386, 125474 (2020). DOI:10.1016/j.surfcoat.2020.125474

[19] Kumar, R. N., & Kumar, D. S., Experimental Investigation of Al2O3-Polyethylene Glycol and TiO2-Polyethylene Glycol Nanofluids Flow through a Minichannel Heat Sink. Asian Journal of Research in Social Sciences and Humanities, 6(9), 1404-1418 (2016). DOI:10.5958/2249-7315.2016.00879.0

[20] Sangwan, K. S., & Kant, G., Optimization of machining parameters for improving energy efficiency using integrated response surface methodology and genetic algorithm approach. Procedia CIRP, 61, 517-522 (2017). DOI:10.1016/j.procir.2016.11.162

[21] Senthilkumar, T. S., Muralikannan, R., Ramkumar, T., & Senthil Kumar, S., Studies of kerf width and surface roughness using the response surface methodology in AA 4032–TiC composites. Proceedings of the Institution of Mechanical Engineers, Part E: Journal of Process Mechanical Engineering, 235(6), 2240-2253 (2021). DOI:10.1177/09544089211041418

[22] Kumar S, Senthil & Pandian, R. &Pitchipoo, Pandian & Senthilkumar, Ts & S.G., Ponnambalam., Investigation of Wear and Wire Electrical Discharge Machining Characteristics of Al-Mg-MoS2 Composites Using Response Surface Method. Journal of Testing and Evaluation. (2022). DOI:10.1520/JTE20220327

[23] Srivastava, M., Rathee, S., Maheshwari, S., & Kundra, T. K., Multi-objective optimisation of fused deposition modelling process parameters using RSM and fuzzy logic for build time and support material. International Journal of Rapid Manufacturing, 7(1), 25-42 (2018). DOI:10.1504/IJRAPIDM.2018.089727

[24] Murkute, P., Pasebani, S., & Burkan Isgor, O. Metallurgical and Electrochemical Properties of Super Duplex Stainless Steel Clads on Low Carbon Steel Substrate produced with Laser Powder Bed Fusion, Scientific Reports, 10(1) (2020). DOI:10.1038/s41598-020-67249-2

[25] Bunaziv, I., Olden, V., & Akselsen, O. M. Metallurgical Aspects in the Welding of Clad Pipelines—A Global Outlook. Applied Sciences, 9(15), 3118 (2019). DOI:10.3390/app9153118v

[26] P. Markopoulos, E.L. Papazoglou, P. Svarnias, P. Karmiris-Obratański, An Experimental Investigation of Machining Aluminum Alloy Al5052 with EDM, Procedia Manufacturing, Volume 41, 2019, Pages 787-794, https://doi.org/10.1016/j.promfg.2019.09.071